Asian Journal of Control, Vol. 16, No. 2, pp. 1–15, May 2014
Published online in Wiley Online Library (wileyonlinelibrary.com) DOI: 10.1002/asjc.754

KINEMATIC NONLINEAR CONTROLLER FOR A MINIATURE HELICOPTER VIA LYAPUNOV TECHNIQUES

Lucio R. Salinas, Emanuel Slawiñski, and Vicente A. Mut

ABSTRACT

This work proposes a kinematic nonlinear controller for an autonomous miniature helicopter that generates saturated reference velocity commands for accurate waypoint trajectory tracking. The control law design is based on a Lyapunov technique with a special choice of the system state equations using spherical coordinates. Stability of the control system is analyzed. Finally, simulation results are presented and discussed, which validate the proposed controller.

Key Words: Lyapunov, nonlinear, UAV, helicopter.

I. INTRODUCTION

In the last decade, unmanned aerial vehicles (UAVs) have attracted a significant interest. UAVs avoid the human risk inherent to human-piloted aerial vehicles, particularly in missions in hostile environments, and they can be smaller and more maneuverable. UAVs have been widely used for military applications, however, the evolution of UAV technologies, the miniaturization of sensors and cameras, and the new advances in communication and control systems point to a wide range of civilian applications, such as aerial photography and cinematography, aerial mapping, environmental monitoring, agriculture and forestry, inspection, law enforcement and security applications, disaster and crisis management, traffic surveillance, communications, and civil engineering [1,2].

Miniature helicopters are a type of rotorcraft-based UAV. They have unique flight capabilities, such as hover, vertical take-off/landing, pirouette, and side-slip, which cannot be achieved by conventional fixed-wing aircraft. One of the core issues in designing a fully autonomous UAV helicopter is to effectively design and implement sophisticated flight control laws. Diverse methods, such as classical PID-controllers and fuzzy logic [3], H_∞ control [4], model predictive control [5], feedforward actions with high-gain and nested saturation feedback [6], neural network with fuzzy logic [7], optimal control techniques [8], robust control [9], and singular perturbation theory [10] have been explored to design autonomous flight control laws for small-scale UAV helicopters.

In [11], the authors proposed a flight control scheme, which is shown in Fig. 1, that consists of three parts: the kernel control (or inner-loop controller), which stabilizes the aircraft and decouples its inputs; the command generator (or outer-loop controller), which generates the flight commands to the inner-loop controller; and the flight scheduling, which produces the flight references to the outer-loop controller according to the respective flight mission. Since the time scale associated with each part of the overall flight control system is hierarchical in nature, the flight control law can be designed in a decentralized fashion [10,12].

In such a context, this work proposes a kinematic nonlinear (outer-loop) controller to guide a miniature helicopter to autonomously track different waypoints. The kinematic controller assumes there is an inner-loop controller that stabilizes and decouples the miniature helicopter so it can track four velocity commands independently: forward/backward, lateral, up/down and heading rate [6,11,13–18]. The controller takes into account the maximum value of the velocity commands the helicopter-inner-loop system can handle to prevent saturation in actuators (from now on, the term helicopter covers the entire helicopter-inner-loop system, unless otherwise specified). The design of the control law is based on the Lyapunov technique, where the state variables are obtained through a transformation of the helicopter's position and heading in spherical coordinates.

This paper is organized as follows. In Section II, a kinematic model of the helicopter is presented. The waypoint tracking control problem and the design of the control laws with their stability analysis are presented in Section III. In Section IV, the simulation results are presented and discussed. Finally, the conclusions are given in Section V.

Manuscript received February 28, 2012; revised August 22, 2012; accepted January 4, 2013.

The authors are with Instituto de Automática (INAUT), Universidad Nacional de San Juan (UNSJ). Av. Libertador San Martín Oeste 1109, J5400ARL, San Juan, Argentina (e-mail: lsalinas,slawinski,vmut@inaut.unsj.edu.ar)

Lucio R. Salinas is the corresponding author (e-mail: lsalinas@inaut.unsj.edu.ar)

This work was partially financed by the UNSJ and the Consejo Nacional de Investigaciones Científicas y Técnicas (CONICET), Argentina.

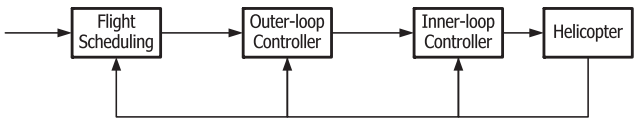

Fig. 1. Schematic diagram of the autonomous flight control law.

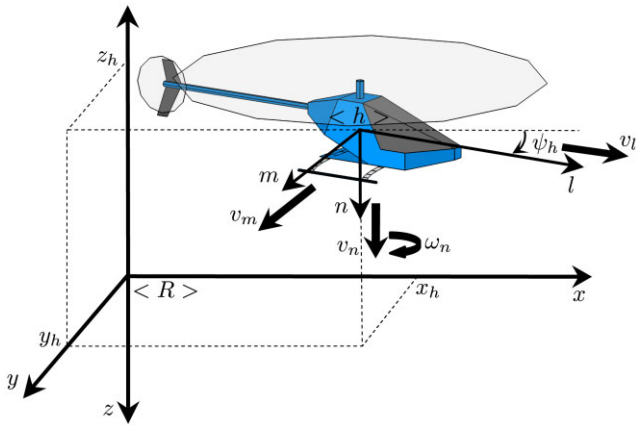

Fig. 2. Helicopter's position and orientation with respect to the frame $< R >$.

II. KINEMATIC HELICOPTER MODEL

Consider a miniature helicopter positioned at any distance with respect to a local North, East, Down (NED) Cartesian coordinate system (frame $< R >$). By convention, the North axis is labelled x, the East y, and the Down z. The helicopter's motion is governed by the combined action of four variables: three linear velocities v_l, v_m, v_n, defined in a rotating right-handed Cartesian coordinate system (helicopter frame $< h >$), and the angular velocity ω_n, as shown in Fig. 2. (The helicopter frame $< h >$ is not a body-fixed frame, but a fictitious frame attached to the helicopter where n is always parallel to z, and l and m lie on the horizontal plane ($z = z_h$). The center of the helicopter frame coincides with the center of gravity of the helicopter.).

Each linear velocity is directed as one of the axes of the frame $< h >$ attached to the helicopter, where v_n always points downward in the same direction as the z axis, and where v_l and v_m point forward and to the right side of the helicopter. The angular velocity ω_n turns the frame $< h >$ around its n axis clockwise (as seen from above the helicopter). Then, the set of kinematics equations, which

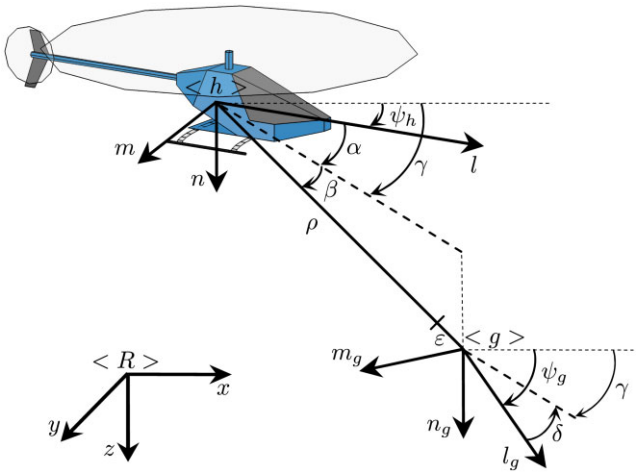

Fig. 3. Helicopter's position and orientation with respect to the goal frame $< g >$.

involves the helicopter's Cartesian position x_h, y_h, z_h and its heading angle ψ_h, are:

$$\begin{cases} \dot{x}_h = v_l \cos\psi_h - v_m \sin\psi_h \\ \dot{y}_h = v_l \sin\psi_h + v_m \cos\psi_h \\ \dot{z}_h = v_n \\ \dot{\psi}_h = \omega_n \end{cases} \tag{1}$$

where x_h, y_h, z_h and ψ_h are all measured with respect to the inertial frame $< R >$.

Now, consider the same miniature helicopter positioned at a non-zero distance with respect to another inertial Cartesian coordinate system (goal frame $< g >$), as displayed in Fig. 3. Making a development similar to [19] but extending it to three dimensions, taking into account the helicopter's position and orientation with respect to the reference frame in terms of its spherical coordinates and the orientation of $< h >$ and $< g >$ with respect to $< R >$, a new set of kinematics equations are obtained:

$$\begin{cases} \dot{\rho} = -v_l \cos\alpha\cos\beta - v_m \sin\alpha\cos\beta - v_n \sin\beta \\ \dot{\alpha} = -\omega_n + v_l \dfrac{\sin\alpha}{(\rho+\varepsilon)\cos\beta} - v_m \dfrac{\cos\alpha}{(\rho+\varepsilon)\cos\beta} \\ \dot{\beta} = v_l \dfrac{\cos\alpha\sin\beta}{(\rho+\varepsilon)} + v_m \dfrac{\sin\alpha\sin\beta}{(\rho+\varepsilon)} - v_n \dfrac{\cos\beta}{(\rho+\varepsilon)} \\ \dot{\gamma} = v_l \dfrac{\sin\alpha}{(\rho+\varepsilon)\cos\beta} - v_m \dfrac{\cos\alpha}{(\rho+\varepsilon)\cos\beta} \end{cases} \tag{2}$$

where

$$\rho + \varepsilon = \sqrt{\tilde{x}^2 + \tilde{y}^2 + \tilde{z}^2},\ \alpha = \gamma - \psi_h,\ \delta = \gamma - \psi_g$$
$$\beta = \tan^{-1}\left(\frac{\tilde{z}}{\sqrt{\tilde{x}^2 + \tilde{y}^2}}\right),\ \gamma = \tan^{-1}\left(\frac{\tilde{y}}{\tilde{x}}\right)$$
$$\tilde{x} = (x_g - x_h),\ \tilde{y} = (y_g - y_h),\ \tilde{z} = (z_g - z_h)$$

with x_g, y_g, z_g and ψ_g as the position and orientation of the goal frame with respect to $< R >$; and ε as an arbitrarily small positive constant.

Note that, since (2) are based on the use of spherical coordinates, they are actually valid only for nonzero values of the distance $\rho + \varepsilon$ (angles α, β, γ are undefined when $\rho + \varepsilon = 0$) and $\beta \neq \pm\frac{\pi}{2}$ (angles α, γ are undefined when $\beta = \pm\frac{\pi}{2}$), thus implying that the generally existing one-to-one correspondence with (1) is actually lost in such singular points.

III. CONTROL DESIGN

Considering the kinematic model of the helicopter given by (2), the waypoint tracking control problem corresponds to the design of a control law that drives the helicopter to the successive goal frames (or waypoints) initially starting from any distance greater than ε (optionally the helicopter can maintain a fixed heading between waypoints). Once the helicopter has reached the first waypoint, it will address the next one and so on. It should be noted that the waypoints are chosen according to $< R >$. The controller must provide the control actions v_l, v_m, v_n, and ω_n such that:

$$\left.\begin{array}{ll} \rho \to 0 & \text{for all flight modes} \\ \alpha \to 0 & \text{for normal flight mode} \\ \alpha \to \delta & \text{for fixed-heading flight mode} \\ \beta \to 0 & \text{for all flight modes} \end{array}\right\} \text{as} \quad t \to \infty \tag{3}$$

One typical problem when implementing a controller is the practical range of the control actions. If not considered in the theoretical design, possible saturation of actuators will occur and, in such cases, the design performance of the control system cannot be guaranteed to be attained. Out of the four variables ρ, α, β, γ, the former is considered critical in terms of saturation because it is not naturally bounded. Therefore, in this section, controller saturation is taken into account without considerable additional calculation effort.

The following is the design of two control laws: a controller for a normal flight mode where the helicopter aligns to the target for a forward flight, and a controller for a fixed-heading flight mode where the helicopter reaches the desired orientation and holds it for the entire flight.

3.1 Control for normal flight mode

Let the helicopter initially be positioned at any distance greater than ε from the goal frame $< g >$ ($\rho(0) > 0$) and assume state variables ρ, α, β, γ to be directly measurable.

Let us consider the following Lyapunov candidate function:

$$V(\rho, \alpha, \beta) = \frac{1}{2}\rho^2 + \frac{1}{2}\alpha^2 + \frac{1}{2}\beta^2 \tag{4}$$

Its time derivative $\dot{V}(\rho, \alpha, \beta)$ along the trajectories of system (2) is given by:

$$\begin{aligned} \dot{V}(\rho, \alpha, \beta) &= \rho\dot{\rho} + \alpha\dot{\alpha} + \beta\dot{\beta} \\ \dot{V} &= \rho[-v_l \cos\alpha\cos\beta - v_m \sin\alpha\cos\beta - v_n \sin\beta] \\ &\quad + \alpha\left[-\omega_n + v_l \frac{\sin\alpha}{(\rho+\varepsilon)\cos\beta} - v_m \frac{\cos\alpha}{(\rho+\varepsilon)\cos\beta}\right] \\ &\quad + \beta\left[v_l \frac{\cos\alpha\sin\beta}{(\rho+\varepsilon)} + v_m \frac{\sin\alpha\sin\beta}{(\rho+\varepsilon)} - v_n \frac{\cos\beta}{(\rho+\varepsilon)}\right] \\ \dot{V}(\rho, \alpha, \beta) &= \dot{V}_1 + \dot{V}_2 + \dot{V}_3 \end{aligned} \tag{5}$$

The first and third terms in (5), corresponding to $\dot{V}_1$ and $\dot{V}_3$, are non-positive definite by setting the three linear velocities v_l, v_m, v_n as follows:

$$\begin{aligned} v_l &= k_l \tanh(k_t\rho)\cos\alpha\left(\cos\beta - \frac{k_n}{k_l}\beta\sin\beta\right) \\ v_m &= k_m \tanh(k_t\rho)\sin\alpha\left(\cos\beta - \frac{k_n}{k_m}\beta\sin\beta\right) \\ v_n &= k_n \tanh(k_t\rho)\beta\cos\beta \\ &\quad + \tanh(k_t\rho)\sin\beta[k_l\cos^2\alpha + k_m\sin^2\alpha] \end{aligned} \tag{6}$$

where k_l, k_m, k_n, and k_t denote some positive constants.

According to the velocities v_l, v_m, v_n in (6), $\dot{V}_2$ in (5) becomes:

$$\dot{V}_2 = \alpha\left[-\omega_n + (k_l - k_m)\frac{\tanh(k_t\rho)}{(\rho+\varepsilon)}\cos\alpha\sin\alpha\right] \tag{7}$$

The last equation is non-positive definite by letting the angular velocity ω_n have the form:

$$\omega_n = k_\omega\alpha + (k_l - k_m)\frac{\tanh(k_t\rho)}{(\rho+\varepsilon)}\cos\alpha\sin\alpha \tag{8}$$

with $k_\omega > 0$.

Then, according to the velocities defined in (6) and (8), (5) takes the following expression:

$$\begin{aligned} \dot{V} &= -(k_l\cos^2\alpha + k_m\sin^2\alpha)\tanh(k_t\rho)\rho \\ &\quad - k_\omega\alpha^2 - k_n\frac{\tanh(k_t\rho)}{(\rho+\varepsilon)}\beta^2 \end{aligned}$$

which results in a negative definite function. This means global asymptotical convergence to zero of the state variables ρ, α, β, thus verifying the control objective:

$$\left.\begin{array}{l} \rho(t) \\ \alpha(t) \\ \beta(t) \end{array}\right\} \to 0 \quad \text{when} \quad t \to \infty \tag{9}$$

Now, it is important to analyze γ in order to know about the helicopter's trajectory orientation.

Remark 1. Let us consider the state equations (2) in the presence of the established feedback laws v_l, v_m, v_n from (6) and ω_n from (8); that is, the closed-loop equations:

$$\begin{cases} \dot{\rho} = -(k_l \cos^2\alpha + k_m \sin^2\alpha)\tanh(k_t\rho) \\ \dot{\alpha} = -k_\omega \alpha \\ \dot{\beta} = -k_n \dfrac{\tanh(k_t\rho)}{(\rho+\varepsilon)}\beta \\ \dot{\gamma} = (k_l - k_m)\dfrac{\tanh(k_t\rho)}{(\rho+\varepsilon)}\cos\alpha\sin\alpha \end{cases} \tag{10}$$

Remark 2. The solution to the second of (10) is

$$\alpha(t) = \alpha_0 e^{-k_\omega t} \tag{11}$$

Considering (11), we can rewrite $\dot{\gamma}$ as follows:

$$\dot{\gamma} = K(\rho)\sin 2\alpha = K(\rho)\sin(2\alpha_0 e^{-k_\omega t}) \tag{12}$$

where $K(\rho) = (k_l - k_m)\dfrac{\tanh(k_t\rho)}{2(\rho+\varepsilon)}$.

Analyzing (12) we can see that, if $k_l = k_m$, $\dot{\gamma} = 0$ for all t and $\gamma(t) = \gamma(0) = \gamma_0$; instead, if $k_l \neq k_m$, $\dot{\gamma} \to 0$ for $t \to \infty$ since ρ, $\alpha \to 0$ according to (9).

Remark 3. Considering that $0 < |K(\rho)| < \dfrac{1}{2}|k_l - k_m|\varepsilon^{-1}$ (for k_t, ρ, $\varepsilon > 0$), the time integral of (12) is bounded by

$$\begin{aligned} &\int_0^t \dot{\gamma}(\tau)\,\mathrm{d}\tau \le \int_0^t |\dot{\gamma}(\tau)|\,\mathrm{d}\tau \\ &\gamma(t) - \gamma_0 < \frac{1}{2}|k_l - k_m|\varepsilon^{-1}\int_0^t \left|\sin[2\alpha_0 e^{-k_\omega t}]\right|\mathrm{d}\tau \\ &\gamma(t) - \gamma_0 < \frac{1}{2}|k_l - k_m|\varepsilon^{-1}\int_0^t |2\alpha_0 e^{-k_\omega t}|\,\mathrm{d}\tau \\ &\gamma(t) - \gamma_0 < |k_l - k_m|\varepsilon^{-1}|\alpha_0|\left[-\frac{e^{-k_\omega t}}{k_\omega}\right]_0^t \end{aligned} \tag{13}$$

then, $\gamma(t)$ is also bounded.

From Remark 2 and Remark 3 we see that $\dot{\gamma} \to 0$ for $t \to \infty$ and that $\gamma(t)$ is bounded.

Next, the parameters k_l, k_m, k_n, k_ω and k_t must be selected in accordance with the maximum values of the velocity commands that the helicopter can handle to prevent saturation of actuators.

We write the equations from (6) and (8) in absolute value and simplify, taking into account the worst-case scenario, to find their upper and lower bounds:

$$\begin{aligned} |v_l| &= \left|k_l \tanh(k_t\rho)\cos\alpha\left(\cos\beta - \frac{k_n}{k_l}\beta\sin\beta\right)\right| \\ |v_l| &< |k_l\cos\beta - k_n\beta\sin\beta| \\ |v_l| &< \max\left\{k_l, \frac{\pi}{2}k_n\right\} \end{aligned} \tag{14}$$

$$\begin{aligned} |v_m| &= \left|k_m \tanh(k_t\rho)\sin\alpha\left(\cos\beta - \frac{k_n}{k_m}\beta\sin\beta\right)\right| \\ |v_m| &< |k_m\cos\beta - k_n\beta\sin\beta| \\ |v_m| &< \max\left\{k_m, \frac{\pi}{2}k_n\right\} \end{aligned} \tag{15}$$

$$\begin{aligned} |v_n| &= |k_n \tanh(k_t\rho)\beta\cos\beta \\ &\quad + \tanh(k_t\rho)\sin\beta[k_l\cos^2\alpha + k_m\sin^2\alpha]| \\ |v_n| &< |k_n\beta\cos\beta + \sin\beta[k_l\cos^2\alpha + k_m\sin^2\alpha]| \\ |v_n| &< 0.5611k_n + \max\{k_l, k_m\} \end{aligned} \tag{16}$$

$$\begin{aligned} |\omega_n| &= \left|k_\omega\alpha + (k_l - k_m)\frac{\tanh(k_t\rho)}{(\rho+\varepsilon)}\cos\alpha\sin\alpha\right| \\ |\omega_n| &< \pi k_\omega + \frac{1}{2}|k_l - k_m|\varepsilon^{-1} \end{aligned} \tag{17}$$

Analyzing (16) we see that the bound is very conservative; hence, the better way to find the real bound is by maximizing the function $f(\beta) = k_n\beta\cos\beta + \sin\beta\max\{k_l, k_m\}$ for $0 < \beta < \dfrac{\pi}{2}$, then

$$|v_n| < \max\{f(\beta)\} \tag{18}$$

Also, (17) is conservative and restrictive; if we assume $k_t \le 1$ (which is a good practice), we get the following less conservative bound:

$$|\omega_n| < \pi k_\omega + \frac{1}{2}|k_l - k_m|k_t \tag{19}$$

Finally, given $|v_{l\max}|$, $|v_{m\max}|$, $|v_{n\max}|$, and $|\omega_{n\max}|$, as the absolute maximum velocities the helicopter can handle, the parameters k_l, k_m, k_n, k_ω, and k_t can be chosen from the following conditions:

$$\begin{aligned} |v_{l\max}| &\ge \max\left\{k_l, \frac{\pi}{2}k_n\right\} \\ |v_{m\max}| &\ge \max\left\{k_m, \frac{\pi}{2}k_n\right\} \\ |v_{n\max}| &\ge \max\{k_n\beta\cos\beta + \sin\beta\max\{k_l, k_m\}\} \\ |\omega_{n\max}| &\ge \pi k_\omega + \frac{1}{2}|k_l - k_m|k_t \end{aligned} \tag{20}$$

with $0 < \beta < \dfrac{\pi}{2}$ and $k_t \le 1$.

3.2 Control for fixed heading flight mode

Let the helicopter be positioned initially at any distance greater than ε from the goal frame $< g >$. If we rearrange (2) in order to take $(\alpha - \delta) = (\alpha - \gamma + \psi_g) = \gamma_h$ as a new state, we get the following new kinematics equations:

$$\begin{cases} \dot{\rho} = -v_l \cos\alpha\cos\beta - v_m \sin\alpha\cos\beta - v_n \sin\beta \\ \dot{\alpha} = -\omega_n + v_l \dfrac{\sin\alpha}{(\rho+\varepsilon)\cos\beta} - v_m \dfrac{\cos\alpha}{(\rho+\varepsilon)\cos\beta} \\ \dot{\beta} = v_l \dfrac{\cos\alpha\sin\beta}{(\rho+\varepsilon)} + v_m \dfrac{\sin\alpha\sin\beta}{(\rho+\varepsilon)} - v_n \dfrac{\cos\beta}{(\rho+\varepsilon)} \\ \dot{\gamma}_h = -\omega_n \end{cases} \tag{21}$$

Let us consider the following Lyapunov candidate function

$$V(\rho, \beta, \gamma_h) = \frac{1}{2}\rho^2 + \frac{1}{2}\beta^2 + \frac{1}{2}\gamma_h^2 \tag{22}$$

Its time derivative $\dot{V}(\rho, \beta, \gamma_h)$, along the trajectories of system (21), is given by:

$$\begin{aligned} &\dot{V}(\rho, \beta, \gamma_h) = \rho\dot{\rho} + \beta\dot{\beta} + \gamma_h\dot{\gamma}_h \\ &\dot{V} = \rho[-v_l \cos\alpha\cos\beta - v_m \sin\alpha\cos\beta - v_n \sin\beta] \\ &\quad + \beta\left[v_l \frac{\cos\alpha\sin\beta}{(\rho+\varepsilon)} + v_m \frac{\sin\alpha\sin\beta}{(\rho+\varepsilon)} - v_n \frac{\cos\beta}{(\rho+\varepsilon)} \right] - \gamma_h\omega_n \\ &\dot{V}(\rho, \alpha, \beta, \gamma_h) = \dot{V}_1 + \dot{V}_2 + \dot{V}_3 \end{aligned} \tag{23}$$

The first and second terms in (23), corresponding to $\dot{V}_1$ and $\dot{V}_2$, are non-positive definite setting the same v_l, v_m, v_n from (6). The third term $\dot{V}_3$ is non-positive definite if the angular velocity is set as follows:

$$\omega_n = k_\omega \gamma_h \tag{24}$$

with $k_\omega > 0$.

Then, according to the velocities defined in (6) and (24), (23) takes the following expression

$$\begin{aligned} \dot{V} = &-(k_l \cos^2\alpha + k_m \sin^2\alpha)\tanh(k_t\rho)\rho \\ &- k_n \frac{\tanh(k_t\rho)}{(\rho+\varepsilon)}\beta^2 - k_\omega\gamma_h^2 \end{aligned}$$

which results in a negative definite function. This means global asymptotical convergence to zero of the state variables ρ, β, γ_h, thus verifying the control objective:

$$\left.\begin{array}{l} \rho(t) \to 0 \\ \alpha(t) \to \delta(t) \\ \beta(t) \to 0 \end{array}\right\} \quad \text{when} \quad t \to \infty \tag{25}$$

As $\psi_h = \gamma - \alpha$ and $\alpha \to \delta = (\gamma - \psi_g)$, then, $\psi_h \to \psi_g$ when $t \to \infty$. Since the waypoints are selected according to $< R >$, we can choose the orientation of each waypoint (ψ_g), hence, the reference for the helicopter's heading.

Now, it is important to analyze α in order to know about the helicopter's orientation with respect to the goal frame.

Remark 4. Let us consider the state equations (21) in the presence of the established feedback laws v_l, v_m, v_n from (6) and ω_n from (24); that is, the closed-loop equations:

$$\begin{cases} \dot{\rho} = -(k_l \cos^2\alpha + k_m \sin^2\alpha)\tanh(k_t\rho) \\ \dot{\alpha} = -k_\omega\gamma_h + (k_l - k_m)\dfrac{\tanh(k_t\rho)}{(\rho+\varepsilon)}\cos\alpha\sin\alpha \\ \dot{\beta} = -k_n \dfrac{\tanh(k_t\rho)}{(\rho+\varepsilon)}\beta \\ \dot{\gamma}_h = -k_\omega\gamma_h \end{cases} \tag{26}$$

Remark 5. The solution to the fourth of (26) is

$$\gamma_h(t) = \gamma_{h0} e^{-k_\omega t} \tag{27}$$

Considering (27), we can rewrite $\dot{\alpha}$ as follows:

$$\dot{\alpha} = -k_\omega\gamma_{h0} e^{-k_\omega t} + K(\rho)\sin 2\alpha \tag{28}$$

where $K(\rho) = (k_l - k_m)\dfrac{\tanh(k_t\rho)}{2(\rho+\varepsilon)}$ is the same as in (12).

Analyzing (28), we can see that, if $k_l = k_m$, its solution is $\alpha(t) = \alpha_0 + \gamma_{h0}(e^{-k_\omega t} - 1)$, which is bounded for all t and converges to $[\alpha_0 - \gamma_{h0}]$; instead, if $k_l \neq k_m$, $\dot{\alpha} \to 0$ for $t \to \infty$ since $\rho \to 0$ according to (25).

Remark 6. From (27), it is possible to see that, in some finite time T, $\gamma_h(t)$ becomes negligible; then, if we consider the worst-case scenario, the time integral from 0 to T of (28) is bounded by:

$$\begin{aligned} &\int_0^T \dot{\alpha}(\tau)\,\mathrm{d}\tau \le \int_0^T |\dot{\alpha}(\tau)|\,\mathrm{d}\tau \\ &\alpha(T) - \alpha_0 < \int_0^T \left|k_\omega\gamma_{h0} e^{-k_\omega t}\right|\mathrm{d}\tau + \int_0^T \frac{1}{2}|k_l - k_m|\frac{\tanh(k_t\rho)}{(\rho+\varepsilon)}\,\mathrm{d}\tau \\ &\alpha(T) - \alpha_0 < |\gamma_{h0}| + \frac{T}{2}|k_l - k_m|\varepsilon^{-1} \\ &\alpha(T) - \alpha_0 < C_1 \end{aligned} \tag{29}$$

Now, after time T, (28) can be described by:

$$\dot{\alpha} \approx \dot{\alpha}_T = K(\rho)\sin 2\alpha_T \tag{30}$$

The latter differential equation does not have an explicit solution; however, based on the fact that $K(\rho)$ is bounded (see Remark 3) and it does not change its sign, we can perform a qualitative analysis to understand how variable α_T behaves.

We start by finding the equilibrium solutions to the differential equation that are the roots of $K(\rho)\sin 2\alpha_T = 0$. The

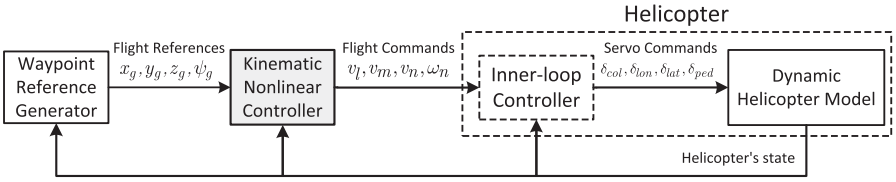

Fig. 4. Block diagram of the simulation system.

case of $k_l = k_m$ was already discussed in Remark 5 and the case when $\rho \to 0$ only occurs for $t \to \infty$, thus it is not part of a finite time analysis (the case when $\rho \to \infty$ is not possible since ρ is bounded, according to (25)). Therefore, the only equilibrium solutions when $\rho > 0$ and $k_l \neq k_m$ are $\alpha_T = n\frac{\pi}{2}$ with $n = \{0, \pm1, \pm2\}$, since $-\pi \leq \alpha_T \leq \pi$.

When $K(\rho)$ is positive ($k_l > k_m$):

- If $\sin 2\alpha_T$ is positive ($0 < \alpha_T < \frac{\pi}{2}$ for α_T starting in Quadrant I or $-\pi < \alpha_T < -\frac{\pi}{2}$ for α_T starting in Quadrant III), $\dot{\alpha}_T$ will be positive too and α_T will grow to $\frac{\pi}{2}$ (from Quadrant I) or to $-\frac{\pi}{2}$ (from Quadrant III).
- If $\sin 2\alpha_T$ is negative ($\frac{\pi}{2} < \alpha_T < \pi$ for α_T starting in Quadrant II or $-\frac{\pi}{2} < \alpha_T < 0$ for α_T starting in Quadrant IV), $\dot{\alpha}_T$ will be negative too and α_T will decrease to $\frac{\pi}{2}$ (from Quadrant II) or to $-\frac{\pi}{2}$ (from Quadrant IV).

When $K(\rho)$ is negative ($k_l < k_m$):

- If $\sin 2\alpha_T$ is positive, $\dot{\alpha}_T$ will be negative and α_T will decrease to 0 (if α_T started in Quadrant I) or to $-\pi$ (if α_T started in Quadrant III).
- If $\sin 2\alpha_T$ is negative, $\dot{\alpha}_T$ will be positive and α_T will increase to π (if α_T started in Quadrant II) or to 0 (if α_T started in Quadrant IV).

The qualitative analysis indicates that α_T will increase or decrease to an equilibrium solution depending on its starting condition in time T and the sign of $K(\rho)$ always staying in the same quadrant.

Joining the results from (29) and the qualitative analysis, the bound of the time integral of (28) can be found:

$$\begin{aligned} &\int_0^t \dot{\alpha}(\tau)\,\mathrm{d}\tau \leq \int_0^t |\dot{\alpha}(\tau)|\,\mathrm{d}\tau \\ &\alpha(t) - \alpha_0 \leq \int_0^T |\dot{\alpha}(\tau)|\,\mathrm{d}\tau + \int_T^t |\dot{\alpha}(\tau)|\,\mathrm{d}\tau \\ &\alpha(t) - \alpha_0 < C_1 + \frac{\pi}{2} \end{aligned} \tag{31}$$

then, $\alpha(t)$ is bounded too.

From remark 5 and remark 6 we see that $\dot{\alpha} \to 0$ for $t \to \infty$ and that $\alpha(t)$ is bounded.

Finally, the parameters k_l, k_m, k_n can be selected following the same first three conditions from (20), and, given a $|\omega_{n\max}|$, k_ω must satisfy $|\omega_{n\max}| \geq \pi k_\omega$.

IV. SIMULATION RESULTS AND DISCUSSION

This section presents the simulation results of the waypoint tracking flight task in the 3D space using the kinematic nonlinear controller designed in the previous section. The goal of the simulations is to test the stability and performance of the proposed controller.

Fig. 4 represents the block diagram of the simulation system. The helicopter model used in the simulation is a very realistic nonlinear dynamic model of a small-scale helicopter found in [20]. The helicopter model considers not-ideal dynamics, such as flapping, drag, and actuator dynamics, and it describes accurately the system's dynamics both for hovering and for low speed translational flights. In the simulations, the helicopter's nominal parameters were used (which refer to MIT's X-Cell .60 acrobatic helicopter).

In order to evaluate the performance of the proposed controller, the helicopter-inner-loop system should be able to independently track four velocity commands: forward, lateral, up/downward, and heading rate. Therefore, we implement a cascaded two-degree-of-freedom (abbreviated as 2DOF) PID velocity tracking architecture similar to [16] as the inner-loop controller (see Fig. 5). It consists of three blocks:

- Velocity Transformation Matrix: it converts the six linear and angular velocities of the dynamic helicopter model expressed in its body-fixed frame (u, v, w, p, q, r) in four velocities (v_l^h, v_m^h, v_n^h, ω_n^h) expressed in the helicopter frame $< h >$ using a rotation matrix that depends on the attitude angles [21]. See Fig. 6 for a visualization of the helicopter frame $< h >$ and the dynamic helicopter body-fixed frame when there is a non-zero pitch angle.
- Inner Velocity Controller: it is a layer of four 2DOF PIDs [22] that generate the reference attitude angles and collective-pedal servo commands.
- Inner Attitude Controller: it is a layer of two PDs that generate the longitudinal and lateral servo commands.

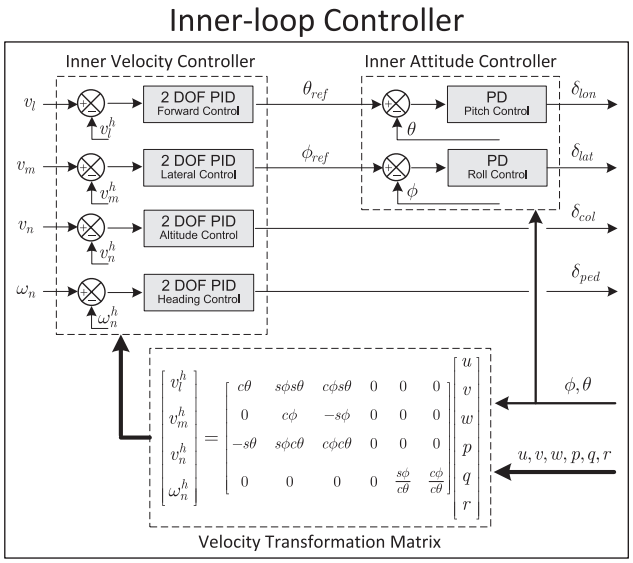

Fig. 5. Description of the inner-loop controller.

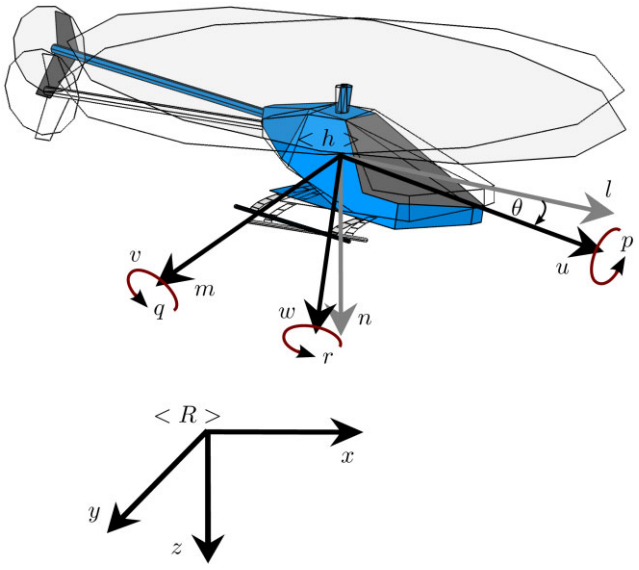

Fig. 6. Helicopter frame < h > and dynamic helicopter body-fixed frame when the pitch angle is non-zero.

Each PID controller has a limit on its output to map the correct reference attitude angles ($\left[-\frac{\pi}{2}, \frac{\pi}{2}\right]$ rad) and the correct servo commands ([−1, 1] rad/rad).

The helicopter also has an internal PID controller to command the throttle input to maintain the desired rotor speed of 167 rad/s.

The flight scheduling consist of a simple waypoint reference generator that gives a flight reference, and it keeps checking the helicopter's position. Once the helicopter has reached the desired waypoint, it gives another waypoint, and so on.

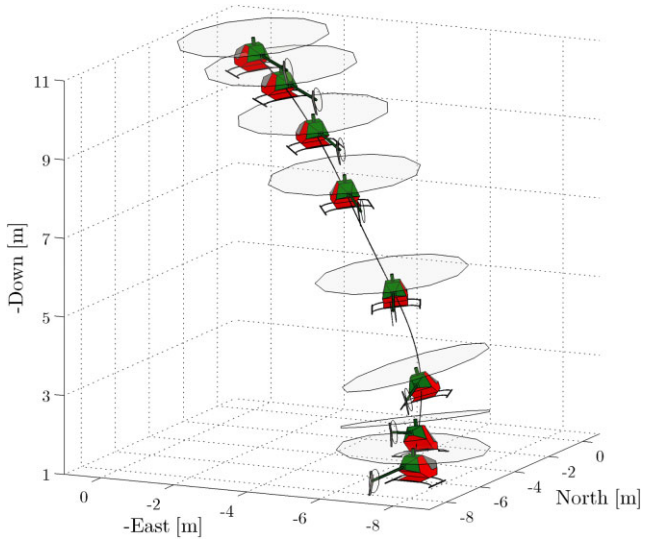

Fig. 7. 3D view of the waypoint stabilization for normal flight mode starting from point [−8.165, 8.165, −8.135].

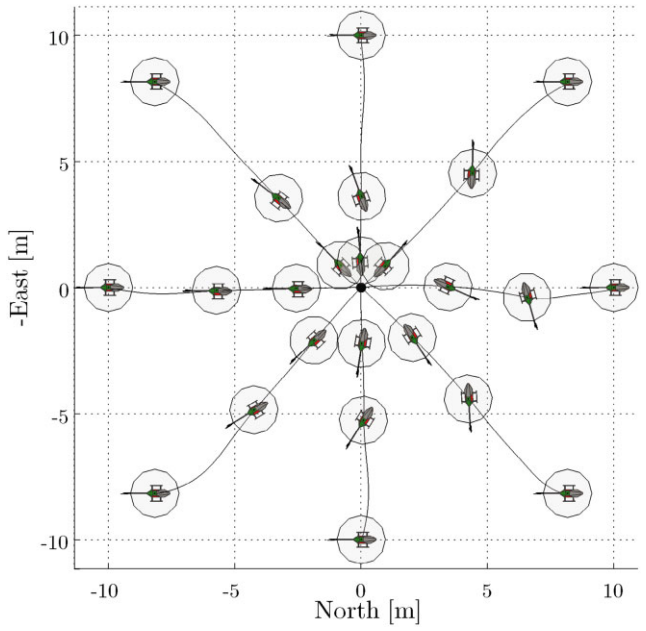

Fig. 8. North-East view of the waypoint stabilization for normal flight mode.

The simulation system was implemented in Visual C++, and a fourth order Runge-Kutta integration method was used, with an integration step of 0.01 seconds. The simulation data were imported into Matlab to generate the figures. The size of the helicopter in the figures is not the real size, it is scaled in order to make the figures more understandable.

In all of the simulations, the waypoints are given in meters according to < R >; also, the following values for the absolute maximum velocities of the helicopter have been considered:

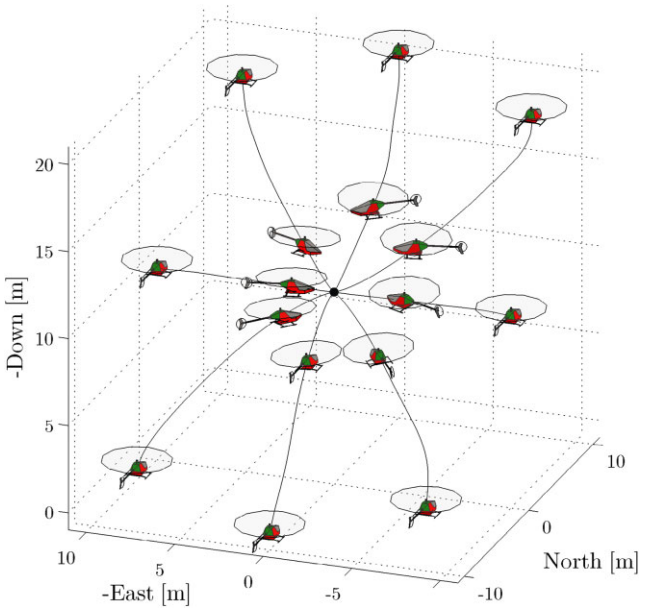

Fig. 9. 3D view of the waypoint stabilization for normal flight mode.

$$|v_{l\max}| = 5\ \text{m/s}, \quad |v_{m\max}| = 5\ \text{m/s}$$
$$|v_{n\max}| = 5\ \text{m/s}, \quad |\omega_{n\max}| = 1\ \text{rad/s}$$

The values chosen for the kinematic controller's parameters are: $k_l = 4.5$, $k_m = 3.5$, $k_n = 1.84$, $k_\omega = \frac{0.95}{\pi}$, $k_t = 0.065$ and $\varepsilon = 0.01$.

4.1 Single waypoint stabilization for normal flight mode

The objective of the simulation is to reach the goal waypoint [0, 0, −10], starting from different points with $\psi_{h0} = 0$. Each flight simulation has a duration of 20 seconds.

Fig. 7, 8, and 9 display the paths that have been traveled by the helicopter during the simulations. Fig. 10 shows that the controlled state variables have an asymptotic behavior towards zero and that the uncontrolled state variable is bounded and its derivative tends to zero. Fig. 11 illustrates the time evolution of the flight commands with the grey line and the helicopter's velocities (v_l^h, v_m^h, v_n^h, ω_n^h) with the black line; therefore, we can verify that there is no signal saturation. The time evolution of the servo commands is indicated in Fig. 12, where there are some signal saturations because of our PID implementation of the inner-loop controller. Figures 10, 11, and 12 correspond to the simulation starting from point [−8.165, 8.165, −8.135].

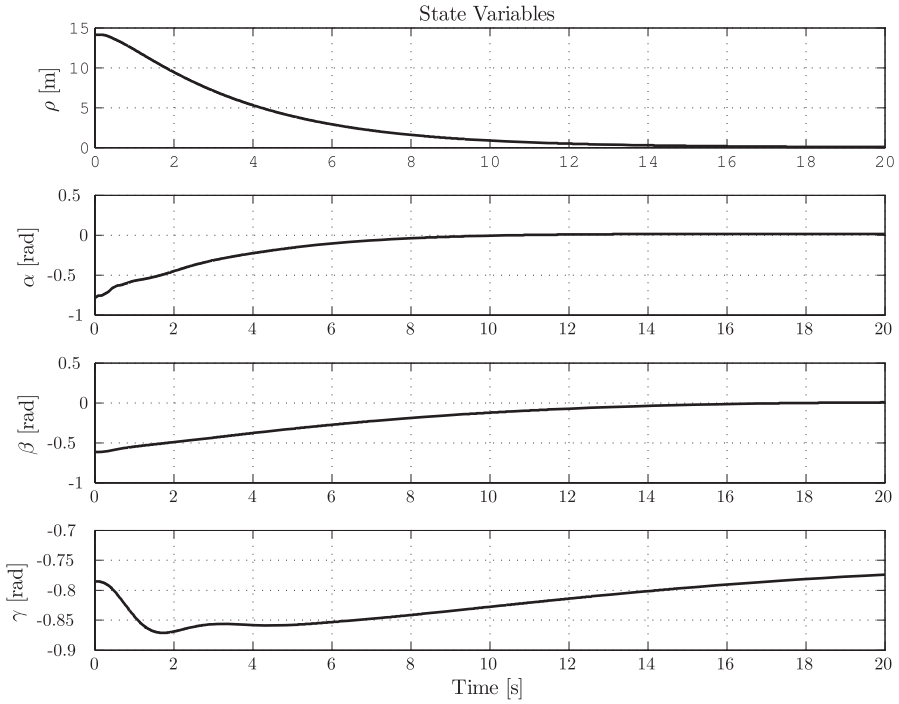

Fig. 10. Time evolution of the state variables ρ, α, β, γ.

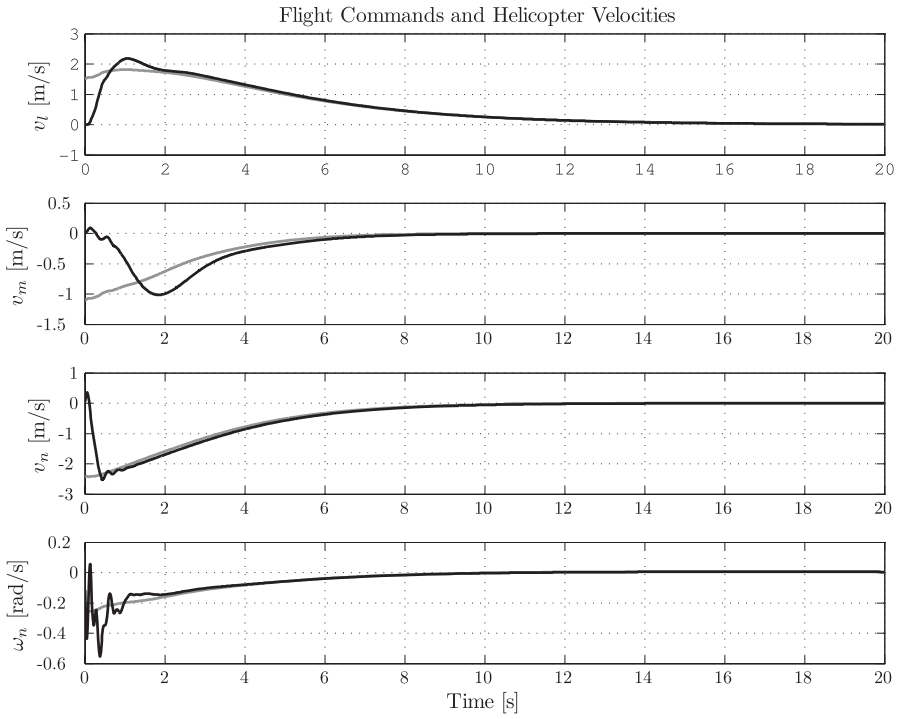

Fig. 11. Time evolution of the flight commands in gray and helicopter's velocities (v_l^h, v_m^h, v_n^h, ω_n^h) in black.

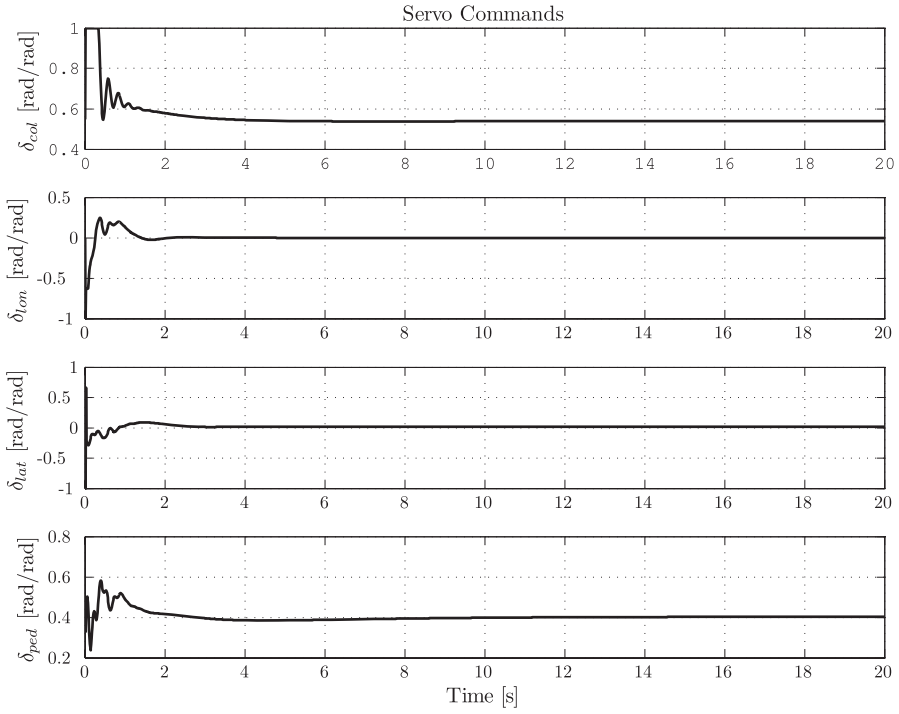

Fig. 12. Time evolution of the servo commands δ_{col}, δ_{lon}, δ_{lat}, δ_{ped}.

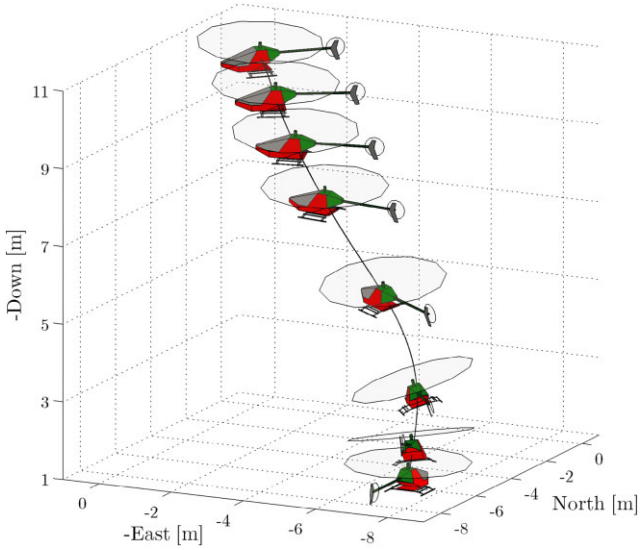

Fig. 13. 3D view of the waypoint stabilization for fixed heading flight mode starting from point [−8.165, 8.165, −8.135].

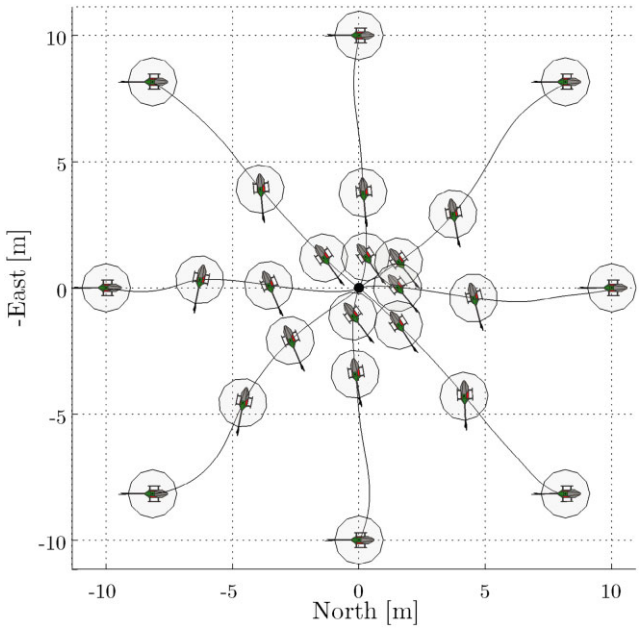

Fig. 14. North-East view of the waypoint stabilization for fixed heading flight mode.

4.2 Single waypoint stabilization for fixed heading flight mode

The objective of the simulation is to reach the goal waypoint [0, 0, −10] and, at the same time, maintain an angle of $-\frac{3}{4}\pi$ measured from the North, starting from different points with $\psi_{h0} = 0$. Each flight simulation has a duration of 20 seconds.

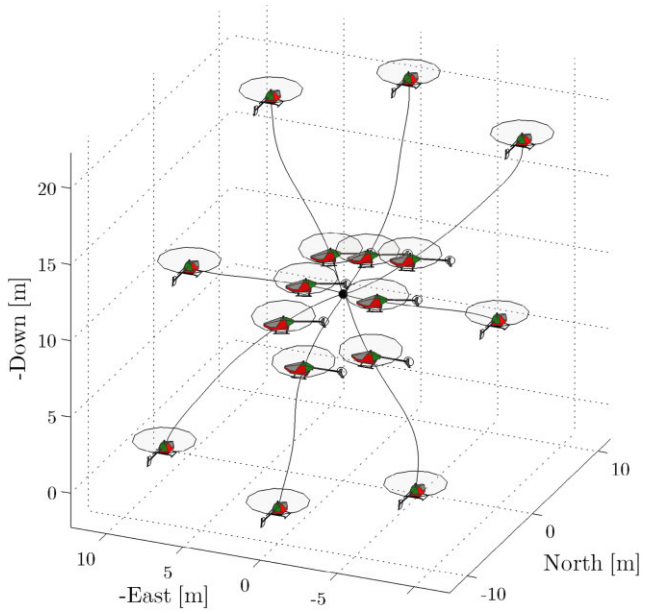

Fig. 15. 3D view of the waypoint stabilization for fixed heading flight mode.

As we can see in Figs 13, 14, and 15, the helicopter approaches the target waypoint while maintaining the desired orientation angle. Figs 16 and 17 illustrate the state variables and the time evolution of the flight commands with the helicopter's velocities, respectively. The time evolution of the servo commands are indicated in Fig. 18.

4.3 Waypoint trajectory tracking

The objective of the simulation is to track the following goal waypoints starting from the point [0, 0, 0] with $\psi_{h0} = 0$:

$$W_1 = [75, -75, -75] \rightarrow W_2 = [75, 75, -75] \rightarrow$$
$$W_3 = [-75, -75, -40] \rightarrow W_4 = [-75, 75, -40] \rightarrow$$
$$W_5 = [-20, 20, 0]$$

If variable ρ is less than 1 meter, the waypoint is considered reached and the waypoint reference generator switches to the next waypoint.

Figs 19 and 20 display the path that has been traveled by the helicopter during the waypoint trajectory tracking simulation. Figs 21 and 22 illustrate the time evolution of the state variables and the flight commands with the helicopter's velocities, respectively. Observing these figures, we reaffirm the acceptable behaviour of the proposed kinematic nonlinear controller.

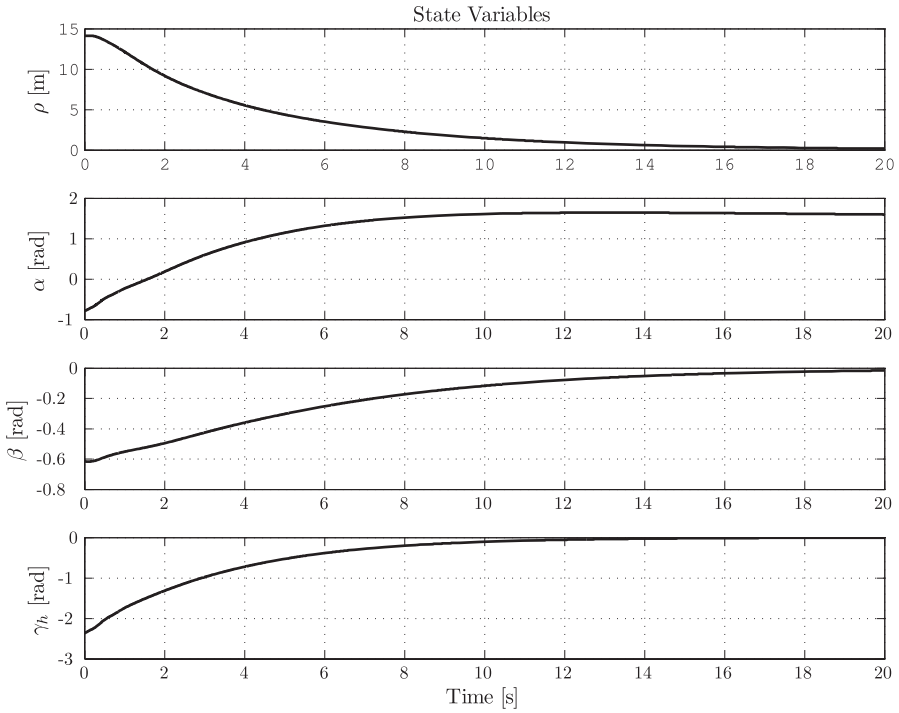

Fig. 16. Time evolution of the state variables ρ, α, β, γ_h.

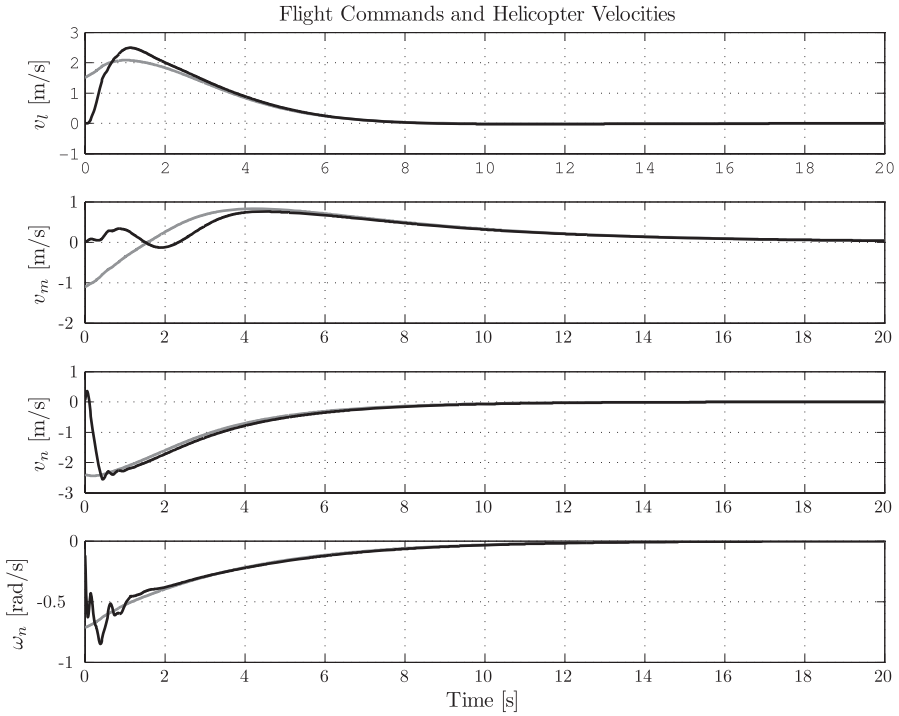

Fig. 17. Time evolution of the flight commands in gray and helicopter's velocities (v_l^h, v_m^h, v_n^h, ω_n^h) in black.

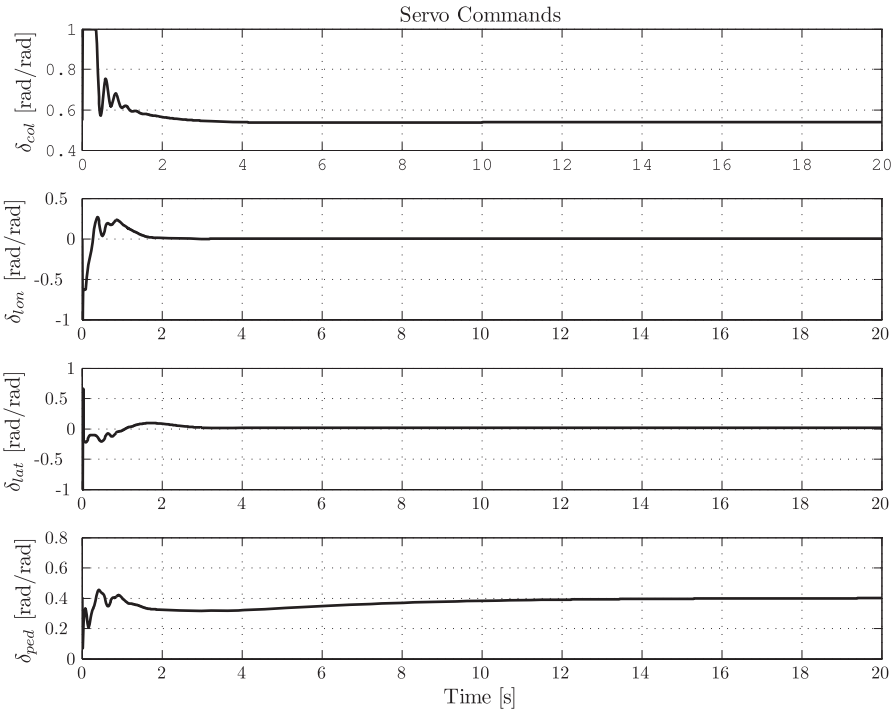

Fig. 18. Time evolution of the servo commands δ_{col}, δ_{lon}, δ_{lat}, δ_{ped}.

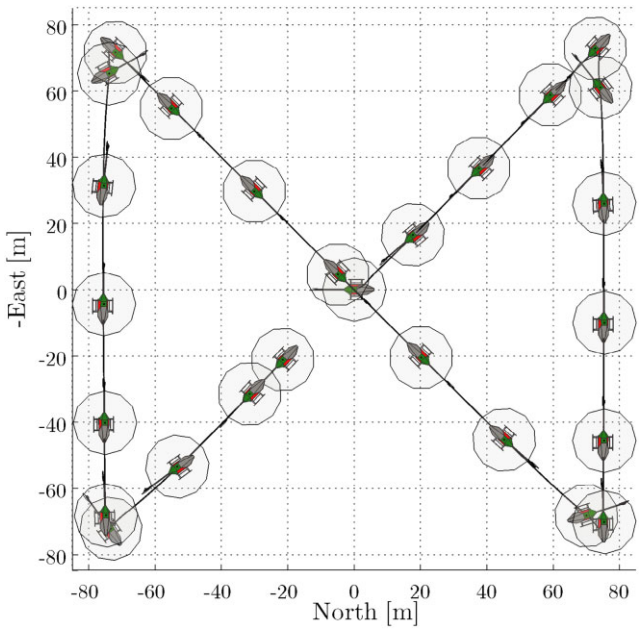

Fig. 19. North-East view of the waypoint trajectory tracking simulation.

V. CONCLUSIONS

In this paper, a kinematic nonlinear controller for an autonomous helicopter has been proposed. The controller has been designed using the Lyapunov technique with a special choice for the system state equations. The simulation's results have proven the controller's ability to globally and asymptotically drive the controlled state variables to zero and simutaneously prevent any saturation in the flight commands. Nevertheless, because of the inner-loop controller implemented in this work, saturation exists in the servo commands. It is worth mentioning that the proposed controller is totally independent of the inner-loop controller as well as the flight scheduling task. Here, the most simple inner-loop controller has been used, a more complex or model-based controller should provide even better results.

For future work, we will investigate the integration of the proposed controller with an impedance controller based on fictitious force to provide obstacle avoidance capability to the miniature helicopter.

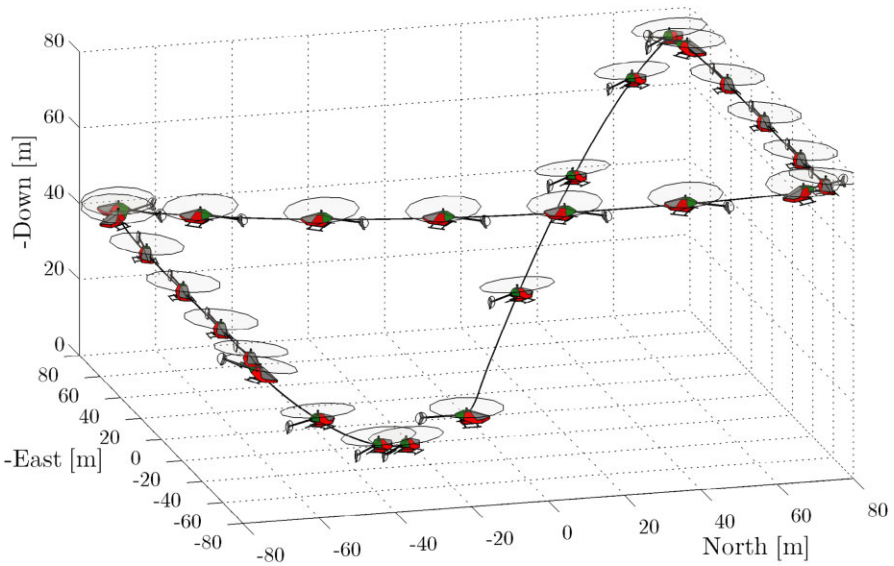

Fig. 20. 3D view of the waypoint trajectory tracking simulation.

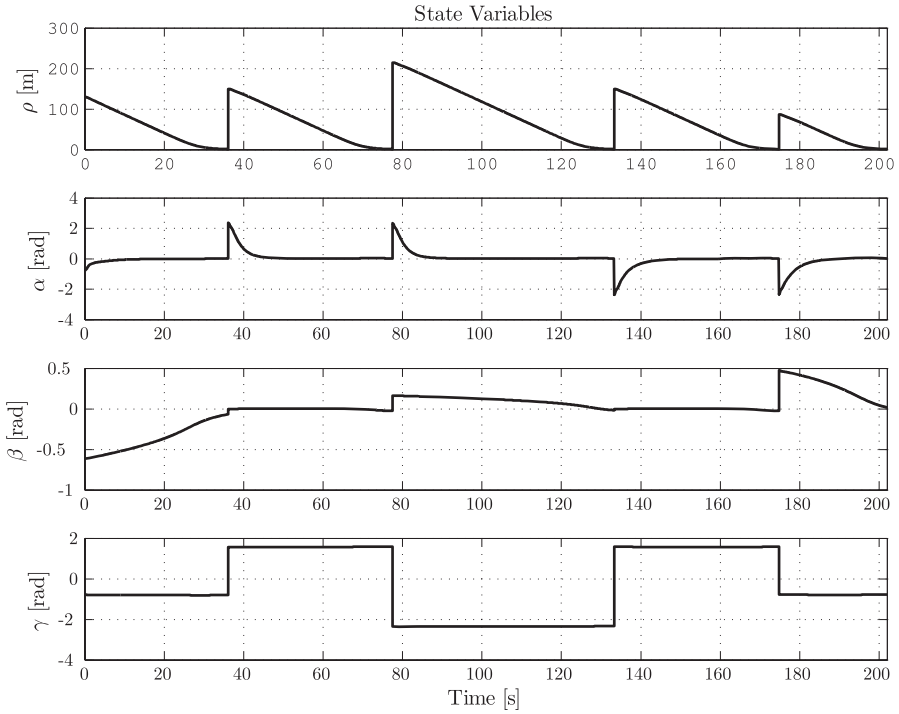

Fig. 21. Time evolution of the state variables ρ, α, β, γ.

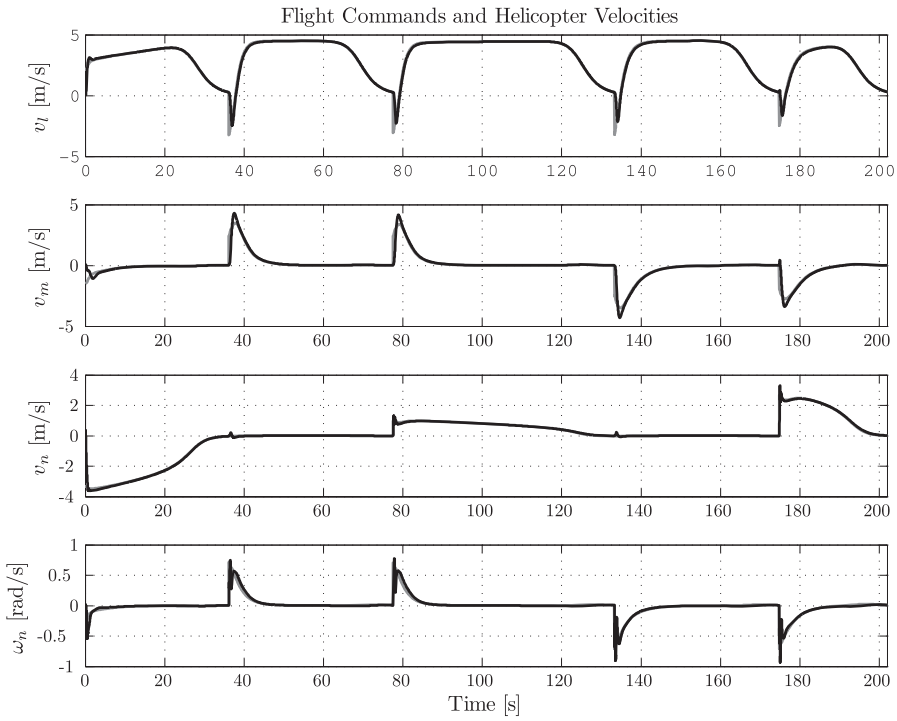

Fig. 22. Time evolution of the flight commands in gray and helicopter's velocities (v_l^h, v_m^h, v_n^h, ω_n^h) in black.

REFERENCES

1. Béjar, M., A. Ollero, and F. Cuesta, Modeling and control of autonomous helicopters. *Advances in control theory and applications*, Springer, Berlin/Heidelberg, pp. 1–29 (2007).
2. Ollero, A. and I. Maza (Eds), *Multiple heterogeneous unmanned aerial vehicles, springer tracts in advanced robotics*, Vol. 37, Springer, Berlin (2007).
3. Castillo, C., W. Alvis, M. Castillo-Effen, W. Moreno, and K. Valavanis, "Small scale helicopter analysis and controller design for non-aggressive flights," *Proc. IEEE Int. Conf. Syst., Man Cybern.*, Vol. 4, pp. 3305–3312 (2005).
4. Civita, M. L., G. Papageorgiou, W. Messner, and T. Kanade, "Design and flight testing of a high-bandwidth h-infinity loop shaping controller for a robotic helicopter," *J. Guid. Control Dyn.*, Vol. 29, No. 1, pp. 485–494 (2006).
5. Shim, D., H. Kim, and S. Sastry, "Decentralized nonlinear model predictive control of multiple flying robots," *Proc. IEEE Conf. Decision and Control*, Vol. 4, pp. 3621–3626 (2003).
6. Marconi, L. and R. Naldi, "Robust full degree-of-freedom tracking control of a helicopter," *Automatica*, Vol. 43, No. 11, pp. 1909–1920 (2007).
7. Zein-Sabatto, S. and Y. Zheng, "Intelligent flight controllers for helicopter control," *Proc. Int. Conf. Neural Networks*, Vol. 2, pp. 617–621 (1997).
8. Budiyono, A. and S. S. Wibowo, "Optimal tracking controller design for a small scale helicopter," *J. Bionic Eng.*, Vol. 4, No. 4, pp. 271–280 (2007).
9. Cai, G., B. Wang, B. M. Chen, and T. H. Lee, "Design and implementation of a flight control system for an unmanned rotorcraft using RPT control approach," *Asian J. Control*, Vol. 15, No. 1, pp. 95–119 (2013).
10. Esteban, S., F. Gordillo, and J. Aracil, "Three-time scale singular perturbation control and stability analysis for an autonomous helicopter on a platform," *Int. J. Robust Nonlinear Control*, (2012). DOI: 10.1002/rnc. 2823.
11. Peng, K., G. Cai, B. M. Chen, M. Dong, K. Y. Lum, and T. H. Lee, "Design and implementation of an autonomous flight control law for a uav helicopter," *Automatica*, Vol. 45, No. 10, pp. 2333–2338 (2009).
12. Bertrand, S., N. Gunard, T. Hamel, H. Piet-Lahanier, and L. Eck, "A hierarchical controller for miniature VTOL UAVs: Design and stability analysis using singular perturbation theory," *Control Eng. Practice*, Vol. 19, No. 10, pp. 1099–1108 (2011).
13. Johnson, E., P. DeBitetto, C. Trott, and M. Bosse, "The 1996 mit/boston university/draper laboratory autonomous helicopter system," *Proc. AIAA/IEEE 15th Digital Avionics Syst. Conf.*, pp. 381–386 (1996).

14. Kim, H. J. and D. H. Shim, "A flight control system for aerial robots: Algorithms and experiments," *Control Eng. Practice*, Vol. 11, No. 12, pp. 1389–1400 (2003).
15. La Civita, M., G. Papageorgiou, W. Messner, and T. Kanade, "Design and flight testing of a gain-scheduled H_∞ loop shaping controller for wide-envelope flight of a robotic helicopter," *Proc. American Control Conf., Denver, Colorado*, Vol. 5, pp. 4195–4200 (2003).
16. Castillo-Effen, M., C. Castillo, W. Moreno, and K. Valavanis, "Control fundamentals of small/miniature helicopters-A survey," In K. Valavanis (Ed.) *Advances in unmanned aerial vehicles*, Springer, The Netherlands, pp. 73–118 (2007).
17. Alvis, W., C. Castillo, M. Castillo-Effen, W. Moreno, and K. Valavanis, "A tutorial approach to small unmanned helicopter controller design for non-aggressive flights," In K. Valavanis (Ed.) *Advances in unmanned aerial vehicles*, Springer, The Netherlands, pp. 119–170 (2007).
18. Cai, G., B. M. Chen, X. Dong, and T. H. Lee, "Design and implementation of a robust and nonlinear flight control system for an unmanned helicopter," *Mechatronics*, Vol. 21, No. 5, pp. 803–820 (2011).
19. Aicardi, M., G. Casalino, A. Bicchi, and A. Balestrino, "Closed loop steering of unicycle like vehicles via lyapunov techniques," *IEEE Robot. Autom. Mag.*,Vol. 2, No. 1, pp. 27–35 (1995).
20. Gavrilets, V. Autonomous aerobatic maneuvering of miniature helicopters. PhD Thesis, Massachusetts Institute of Technology. Dept. of Aeronautics and Astronautics, Cambridge, MA, (2003).
21. Cook, M. *Flight dynamics principles*. Elsevier, Waltham, MA, (2007).
22. Araki, M., and H. Taguchi, "Two-degree-of-freedom PID controllers," *Int. J. Control Autom. Syst.*, Vol. 1, pp. 401–411 (2003).

Lucio R. Salinas was born in San Juan, Argentina, on November 7, 1982. He graduated in electronic engineering and received Ph.D. degree in control systems engineering from the National University of San Juan (UNSJ), Argentina, in 2008 and 2013, respectively. He holds a scholarship at National Council of Scientific and Technical Investigations of Argentina (CONICET). His research interests are on robotics, teleoperation systems, unmanned aerial vehicles, man-machine systems, and software development.

Emanuel Slawiñski was born in Chubut, Argentina, on November 5, 1975. He graduated from National University of San Juan (UNSJ), San Juan, Argentina, where he received Doctoral Degree on Control Systems Engineering, in 2006. Currently, he is Researcher at National Council of Scientific and Technical Investigations of Argentina (CONICET) and he is Professor at UNSJ in the careers of electronic engineering as well as Ph.D. His areas of interest are teleoperation systems, human factors, human–robot interaction and software development.

Vicente A. Mut was born in San Juan, Argentina, on December 1, 1962. He graduated with diploma of honor to the best average as Electronic Engineer in National University of San Juan (UNSJ), San Juan, Argentina, in 1987. Between 1990 and 1995, he developed their doctorate in Control Systems Engineering at UNSJ. Currently, he is Professor at UNSJ, developing research activities and teaching at the graduate and postgraduate programs at Automatics Institute and Department of Electronics and Automatics. He is also Independent Researcher at National Council of Scientific and Technical Investigations of Argentina (CONICET). His research interests are on robotics, manufacturing systems, adaptive control and artificial intelligence applied to automatic control.